FUNDAMENTALS & APPLICATIONS

CHEMELECTROCHEM

ANALYSIS & CATALYSIS, BIO & NANO, ENERGY & MORE

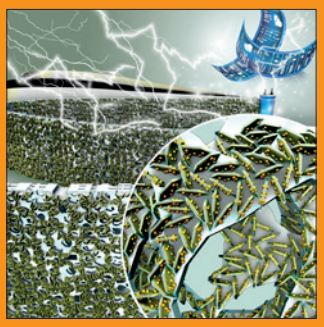
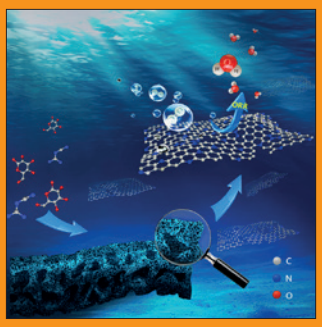
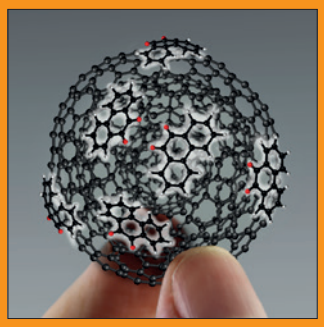
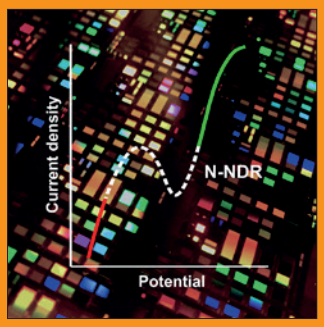

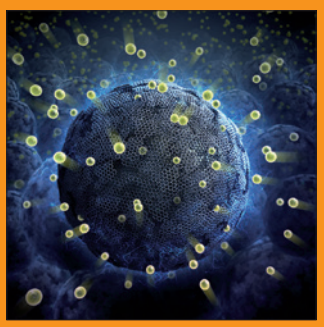



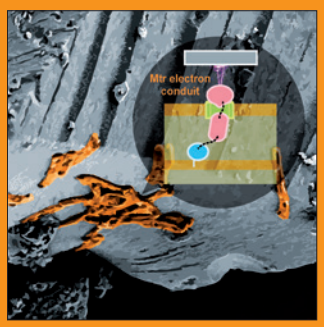

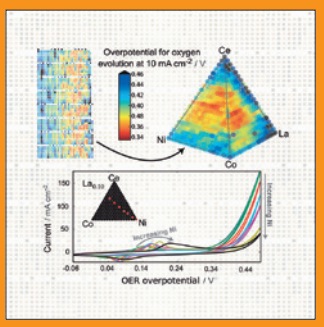

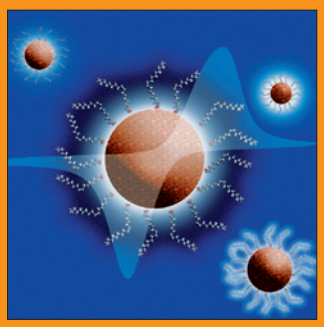
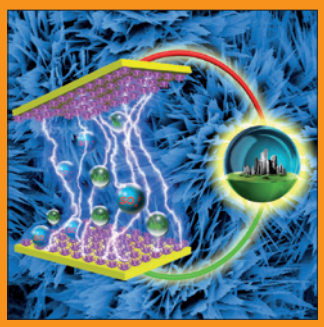
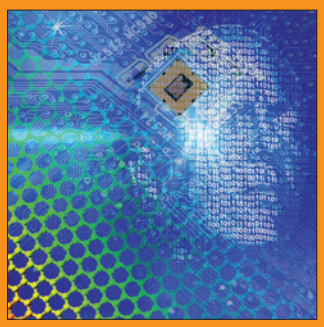

Reprint

A Journal of

WILEY-VCH

www.chemelectrochem.org

ChemPubSoc Europe

ChemPubSoc Europe

DOI: 10.1002/celc.201700100

CHEMELECTROCHEM Articles

Graphene-Encapsulated Copper tin Sulfide Submicron Spheres as High-Capacity Binder-Free Anode for Lithium-Ion Batteries

Lin Fu,[a, b] Xiaogang Wang,*[a] Jun Ma,[a] Chuanjian Zhang,*[a] Jianjiang He,[a, b] Hongxia Xu,[a] Jingchao Chai,[a, b] Shizhen Li,[a, c] Fenglian Chai,[a, c] and Guanglei Cui*[a]

Sn-based sulfides are potential anode materials for lithium-ion batteries (LIBs); nevertheless, they typically suffer from poor cycle stability resulted from the huge volume variation during lithium-ion insertion and extraction. Herein, we successfully fabricated the multiphase $Cu_2Sn_3S_7/Cu_2SnS_3/SnS_2$ (CTS) submicron spheres uniformly incorporated with reduced graphene oxide nanosheets (CTS@RGO). This binder-free hybrid CTS@RGO paper exhibits favorable capacity retention as an anode of LIBs (965 mAh g^{-1} after 300 cycles at current density of 500 mA g^{-1}), as well as better rate capability and high initial coulombic efficiency compared with that of a pristine CTS anode. The enhanced electrochemical performance can be ascribed to the introduction of graphene as a buffer to accommodate large volume changes and to maintain structural integrity of electrode.

1. Introduction

Electrical vehicle and portable electronic markets are experiencing explosive growth, which increase the global demands for lithium-ion batteries (LIBs) with high energy density.[1] The energy density of LIBs are mainly determined by the employed material systems. Currently, the low capacity of commercial graphite anode (LiC_6, 372 mAh g^{-1}) is a great hinder for developing LIBs with high energy density.[2] Therefore, it is necessary to develop novel anode materials with high theoretical capacities to improve the LIBs performances. In recent years, transition sulfide materials possessing high capacity (exceeding 700 mAh g^{-1}) have been studied as anode materials for LIBs.[3]

Sn-based anode materials are known for their high capacities (994 mAh g^{-1} for Sn) and environmental-friendly merits, which have been extensively explored last decade.[4] However, up to now, Sn-based compounds are still suffering from poor cycle stability for the huge volume variation during lithium insertion and extraction process.[5] In order to address this issue, one of the most-effective approaches is to prepare Sn-based materials with nanostructure, which can efficiently accommodate the enormous volume changes and thus improve the cycling performance.[6] In addition, the introduction of carbon materials as buffer for Sn volume expansion is also considered as an effective route to enhance the cycling stability of Sn-based anodes.[7] It is worth noting that graphene is always employed as a helpful additive for its superior mechanical and chemical stability, as well as excellent electrical conductivity.[8] In particular, various Sn-based compound/reduced graphene oxide (RGO) composites as anode materials for LIBs had been prepared and exhibited excellent electrochemical performance.[9]

On the other hand, single transition metal oxides and sulfides are abundantly investigated as a solution to overcome the poor cycling performance of Sn used in LIBs.[4b,10] And the binary transition metal sulfide shows better electronic conductivity in comparison with its single metal counterparts.[11] More importantly, the in-situ formation of inactive metal, such as Cu, can as inert matrix to mitigate the volume changes during the cycling process.[12] In recent years, Sn-based binary metal sulfide ($MSnS_x$, M=Cu, Fe et al.) anodes have been reported and exhibited superior electrochemical performance.[13] Nevertheless, the presence of inactive metal leads to the decrease of theoretical specific capacity of materials. Therefore, it is highly challenged and desirable to reduce the stoichiometric of inactive metal in Sn-based binary metal sulfide, and then enhance its theoretical specific capacity. Moreover, the existence of electrochemical inert additive of binder may also lead to a series of side reactions (e.g. reduce electronic conductivity and block Li^+ diffusion channel) and finally decrease the electrochemical performance.[14] Therefore, the fabrication of binder-free and graphene-standing composites electrodes is an effective method to solve these problems.

In this work, a self-standing and binder-free composite of $Cu_2Sn_3S_7/Cu_2SnS_3/SnS_2$ (CTS) submicron spheres incorporated

[a] L. Fu, X. Wang, J. Ma, C. Zhang, J. He, H. Xu, J. Chai, S. Li, F. Chai, Dr. G. Cui
Qingdao Industrial Energy Storage Research Institute
Qingdao Institute of Bioenergy and Bioprocess Technology
Chinese Academy of Sciences
No.189 Songling Road, Laoshan District, Qingdao, 266101 (P.R. China)
E-mail: wangxg@qibebt.ac.cn
zhangcj@qibebt.ac.cn
cuigl@qibebt.ac.cn
[b] L. Fu, J. He, J. Chai
University of Chinese Academy of Sciences
No.19 Yuquan Road, Shijingshan District, Beijing, 100190 (P. R. China)
[c] S. Li, F. Chai
Qingdao University of Science and Technology
No.53 Zhenzhou Road, Shibei District, Qingdao, 266042 (P. R. China)

Supporting information for this article is available on the WWW under http://dx.doi.org/10.1002/celc.201700100

with RGO nanosheets (CTS@RGO) was successfully prepared as anode material for LIBs. And the lithium storage behavior of the CTS @RGO composite as anode material was investigated. Benefited from the unique structure feature, the hybrid CTS@RGO paper exhibited favorable capacity retention (965 mAh g^{-1} after 300 cycles), batter rate capability and high initial coulombic efficiency (82.36%).

2. Results and Discussion

The preparation process of the hybrid CTS@RGO paper is schematically shown in Figure 1. The GO nanosheets and CuSn

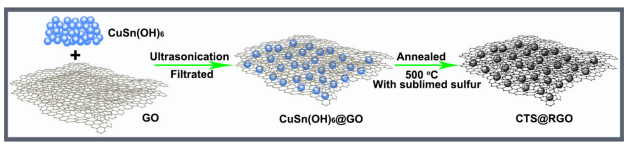

Figure 1. Schematic diagram for the preparation of the hybrid CTS@RGO paper.

$(OH)_6$ submicron spheres (Figure S1 and S3a) were uniformly dispersed into distilled water by ultrasonication. Afterwards, the suspension was then filtrated under the assistance of vacuum through a hydrophilic membrane, followed by lyophilization. The hybrid CTS@RGO paper were prepared by annealing CuSn $(OH)_6$@GO paper with sublimed sulfur under argon atmosphere.

XRD technology was employed to identify the composition and structure of the as-synthesized samples. As depicted in Figure 2, the coincidence of diffraction peak for CTS and

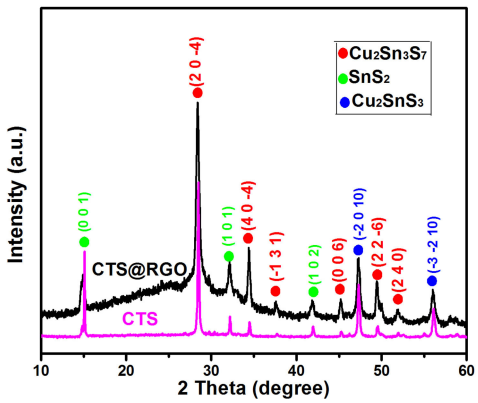

Figure 2. XRD patterns of the hybrid CTS@RGO paper and CTS powder.

CTS@RGO indicates that the introduction of graphene does not alter the crystal structure of the samples. Moreover, for the CTS@RGO sample, the broad diffraction peak at 2θ ranges of 20~30° was attributed to the carbon from the graphene.[15] From the XRD patterns, it can be concluded that the main phase of the CTS and CTS@RGO samples is monoclinic $Cu_2Sn_3S_7$ (PDF NO. 39-0970). Peaks indexed to Cu_2SnS_3 (PDF NO. 27-0198) and SnS_2 (PDF NO. 23-0677) were also observed in the XRD patterns. As reported in the published paper, in the process of preparation of copper tin sulfide film, the $Cu_2Sn_3S_7$ began to become the main phase with three other impurity phases ($Cu_{10}Sn_2S_{13}$, Cu_4SnS_4, SnO_2) at 500 °C.[16] Similarly, for the CTS and CTS@RGO samples, SnS_2 and Cu_2SnS_3 were also formed during the annealing preparation process. In order to check the graphene content of the hybrid CTS@RGO paper, TGA measurement was carried out and the result was displayed in Figure S2. Specifically, graphene and sulfur in the composite were oxidized to CO_2 and SO_2, respectively. Finally, only CuO and SnO_2 remained after test. Therefore, based on the residual weight calculation, the graphene content of hybrid CTS@RGO paper is ca. 9.74%.

The morphology of the as-synthesized materials was evaluated by FESEM and FETEM. For the hybrid CTS@RGO paper, as shown in Figure 3a, the sphere morphology of the

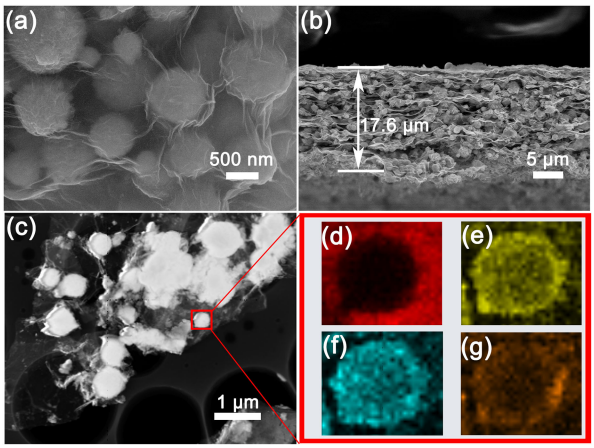

Figure 3. a, b) SEM and c) STEM images of the hybrid CTS@RGO paper. d–g) EDS elemental mapping of C, Cu, Sn, and S, respectively.

CTS maintained well. The SEM image revealed that CTS spheres were incorporated well with the conductive graphene layers. However, for the CTS, the sample aggregated together and formed a bulk (Figure S3b). From the cross-sectional SEM images of hybrid CTS@RGO paper in Figure 3b, we can see that the thickness of this paper is about 17.6 μm after filtration and sulfuration treatment. More importantly, the CTS submicron spheres uniformly embedded in the graphene nanosheets forming a sandwich configuration. This sandwich structure is regarded as an effective route to limit the volume expansion of active materials during lithium insertion.[17] From the STEM image in Figure 3c, it can be seen that the CTS spheres and graphene nanosheets well connect with each other, which is beneficial to the electron transfer. The EDS elemental mapping of single CTS@RGO sphere in the area marked of STEM image is shown in Figure 3d–g. The results indicate the uniform distribution of C, Cu, Sn and S elements in the CTS@RGO composite. In addition, the appearance of the hybrid CTS@RGO paper is displayed in Figure S3c, which shows a good integrity for binder-free electrode fabrication.

Further structure features and surface elemental chemical states of the hybrid CTS@RGO paper were evaluated by Raman spectra and X-ray photoelectron spectra (XPS). As shown in Figure 4a, Raman spectra exhibit two characteristic peaks of D

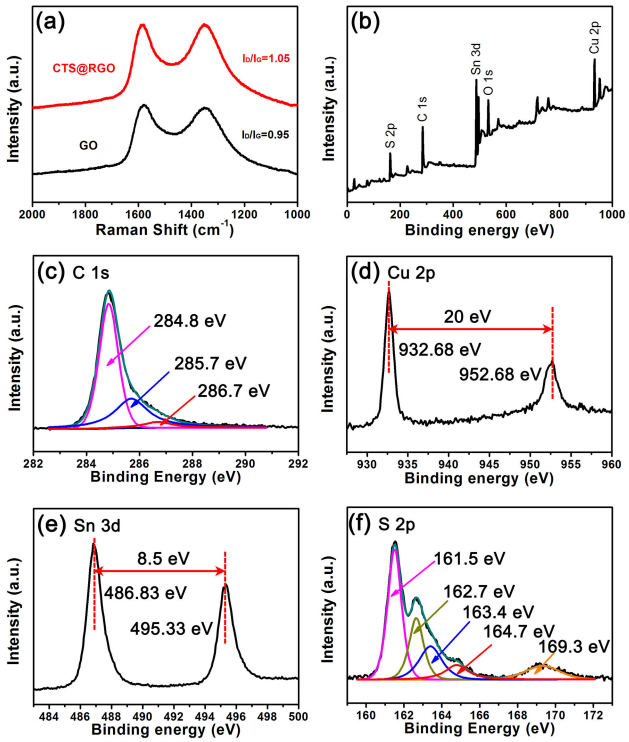

Figure 4. a) Raman spectra of GO and hybrid CTS@RGO paper. b) XPS spectra of hybrid CTS@RGO paper, and corresponding high-resolution XPS spectra of c) C 1s, d) Cu 2p, e) Sn 3d, and f) S 2p.

bands at about 1352 cm^{-1} and G bands at about 1579 cm^{-1} for CTS@RGO, and the same positions of D bands and G bands are observed for pure GO.[18] And the intensity ratio (I_D/I_G) was 0.95 based on GO Raman curves, while this ratio value increased to 1.05 for CTS@RGO, this is because the GO in $CuSn(OH)_6$@GO sample had been partial reduced during the sulfuration process leading to the decreasing of average size and the increasing of quantity of the sp^2 domain.[19] Figure 4b shows the full-scale XPS spectra of the hybrid CTS@RGO paper, which obviously indicates the hybrid CTS@RGO paper consisting of copper (Cu), tin (Sn), sulfide (S) and carbon (C). And the O 1 s peaks at about 532 eV may be attributed to the residual oxygen-containing functional groups of RGO for CTS@RGO.[20] As shown in Figure 4c, the high-resolution spectrum of C 1s in CTS@RGO exhibits a major C–C/C=C and a minor C–O peaks at 284.8 eV and 286.7 eV, respectively, while the particular peak located at 285.7 eV indicating the presence of C–S bond.[21] In the high resolution XPS spectra for Cu 2p, two sharp characteristic peaks of the Cu $2p_{3/2}$ and Cu $2p_{1/2}$ at 932.68 eV and 952.68 eV can be clearly observed in Figure 4d, indicating a 20.0 eV split of Cu (I).[22] There are also two main peaks at 486.83 eV and 495.33 eV (8.5 eV of peak splitting) related to the Sn $3d_{5/2}$ and Sn $3d_{3/2}$ bands detected in the XPS spectra for Sn 3d as shown in Figure 4e, which are in agreement with literature values of Sn (IV).[12a] For the XPS spectra of S in Figure 4f, the main peak located at 161.5 eV and the shoulder peak at 162.7 eV are due to the $2p_{3/2}$ and $2p_{1/2}$ orbital of metal sulfide.[12a,22] In addition, the three different characteristic peaks with binding energy of 163.4 eV, 164.7 eV and 169.3 eV corresponding to S–C, S–C and -SO_3H peaks, respectively, confirms the existence of S-doped graphene.[20,21b]

The lithium storage properties of the hybrid CTS@RGO paper as anode materials of LIBs were investigated by CV and galvanostatic charge/discharge cycling measurements. As depicted in Figure 5a, the CV measurement for the hybrid

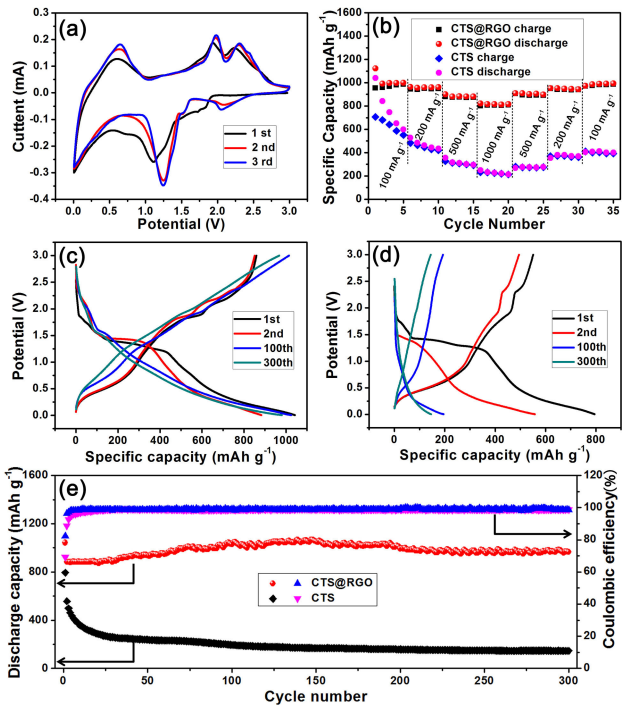

Figure 5. a) Cyclic voltammogram of the hybrid CTS@RGO paper at a scan rate of 0.2 mV s^{-1}. b) Rate capability of the hybrid CTS@RGO paper and CTS at different current densities (from 100 mA g^{-1} to 1000 mA g^{-1}). Charge/discharge curves of the c) hybrid CTS@RGO paper and d) CTS at the current density of 500 mA g^{-1}. e) The cycle performances of the hybrid CTS@RGO paper and CTS at the current density of 500 mA g^{-1}.

CTS@RGO paper was applied at a scanning rate of 0.2 mV s^{-1} for the first three cycles. And it can be seen that the CV curves of hybrid CTS@RGO paper reveal well-defined redox peaks, which is similar to the CV curves of Sn-based binary metal sulfides.[4d,23] In the first cathodic scan (lithium insertion), a well-defined broad peak at 1.1 V accompanied by the weak at 1.72 V were clearly observed, which can be attributed to the multi-step conversion of CTS@RGO with lithium ion to form Cu, Sn and amorphous Li_2S.[4d] The cathodic peaks transfer to around 1.25 V and 2.1 V in the following second and third sweep, which may be ascribed to the formation of metallic Cu and Sn during the subsequent cycles.[23a] A cathodic peak in the regions of 0.5–0.005 V and an anodic peak located about at 0.6 V were assigned to the alloy/dealloy reactions of Li^+ and Sn.[4d,23b] In

the anodic scan (lithium extraction), a pair of distinct current peaks centered at about 1.9 V and 2.3 V can be ascribed to the oxidation of Sn and Cu, respectively.[23c,24] The oxidation and reduction voltages remained unvaried in the subsequent cycles after first cycle, indicating good reversibility and cycling stability. The phase evolution of CTS@RGO electrode upon Li^+ insertion was investigated by ex situ XRD, as shown in Figure S4. Note that the diffraction peaks absence of the lithiated products of Li_2S and Li–Sn alloy phases can be attributed to the poor crystallinity or amorphous of these lithiated products.[11a,25] At the discharge potential of 1.0 V, the diffraction peaks of CTS appeared with Cu, Sn and Li_2S phases formed. When discharged to 0.005 V, all the peaks of Sn disappeared completely, indicating the formation of Li–Sn alloys. The results are corresponding to the above CV data.

Figure 5b illustrates the charge/discharge rate capability of the hybrid CTS@RGO paper and pristine CTS at different current densities between 100 and 1000 mA g^{-1}. Surprisingly, the hybrid CTS@RGO paper obviously display a high rate capability compared with pristine CTS. Even at a relatively high current density of 1000 mA g^{-1}, the hybrid CTS@RGO paper deliver a capacity of 805 mAh g^{-1}, which is much higher than the capacity of 226 mAh g^{-1} for CTS. The superior rate performance of the binder-free hybrid CTS@RGO paper was attributed to the existence of graphene improves electronic conductivity.[26] In order to further understand the advantage of graphene, the electrochemical impedance spectra of the CTS@RGO and CTS electrodes were analyzed. Whether before cycling or after 50 cycles, the impedance value of the CTS@RGO is significantly lower than that of CTS (Figure 6), which was ascribed to the

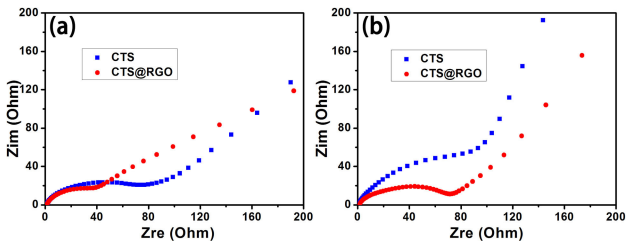

Figure 6. Electrochemical impedance spectra of the hybrid CTS@RGO paper and CTS electrodes a) before cycling and b) after 50 cycles.

highly conductive graphene. The galvanostatic charge/discharge voltage profiles of the hybrid CTS@RGO paper for the 1st, 2nd, 100th and 300th cycles at a constant current density of 500 mA g^{-1} are shown in the Figure 5c. It can be seen that all slope regions are in agreement with above CV result. Compared with Figure 5c, except the first cycle, the charge/discharge plateau of the pristine CTS at a constant current density of 500 mA g^{-1} are greatly changed (Figure 5d), implying that the introduction of graphene can enhanced stable reaction of active materials during the cycling process.

Charge/discharge cycling stability is the focus on Sn-based anode materials. As displayed in Figure S5, the RGO electrode exhibits a high reversible capacity of 443 mAh g^{-1} was obtained after 300 cycles at a constant current density of 500 mA g^{-1}. Based on the graphene content in the electrode of hybrid CTS@RGO paper, its RGO offers a capacity of ca. 43 mAh g^{-1}. The pristine CTS only exhibited an initial discharge capacity of 794.7 mA g^{-1}, with an initial CE of 69.31% at a constant current density of 500 mA g^{-1}. Furthermore, the discharge capacity of pristine CTS rapidly decayed to 146 mA g^{-1} after 300 cycles with low capacity retention rate of 18.4%, whereas the hybrid CTS@RGO paper showed an excellent cycling stability. The discharge capacity of CTS@RGO paper in the initial cycle was 1043.1 mAh g^{-1} at the same current density (500 mA g^{-1}). The hybrid CTS@RGO paper presented an initial CE of 82.36%, which is much higher than that of the majority Sn-based anode materials for the lithium storage.[10] The higher CE of the hybrid CTS@RGO paper may be ascribed to the binder-free electrode fabrication method due to the existence of binder may also lead to a series of side reactions and finally decrease the CE.[14] In addition, for the hybrid CTS@RGO paper, a high discharge capacity of 965 mAh g^{-1} was retained after 300 cycles (Figure 5e), which could be attributed to the graphene existed in the composite significantly improving cycling stability of the CTS by supplying buffer for volume variation. In order to verify this effect, the morphology variations of CTS and hybrid CTS@RGO paper anodes after 100 cycles at a current density of 200 mA g^{-1} were examined by FESEM. The results (Figure 7a)

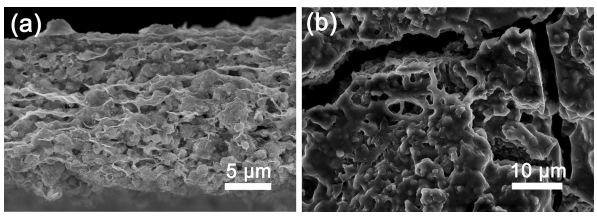

Figure 7. SEM images of a) the hybrid CTS@RGO paper and b) CTS anodes after 100 cycles at a current density of 200 mA g^{-1}.

show that the cycled hybrid CTS@RGO paper did not lead to the pulverization of CTS submicron spheres, while the CTS electrode with pristine uniform distributed CTS particles cracked and aggregated after 100 cycles (Figure 7b). The maintenance of structure integrity and volume of hybrid CTS@RGO paper benefited from the superior physical stability of the sandwich structure electrode. As shown in Figure 5e, it also can be found that the hybrid CTS@RGO paper show a phenomenon of capacity rise from 2nd to 140th cycle, which was possibly ascribed to pseudocapacitance effect caused by the interfacial Li storage mechanism.[27] In addition, a reversible capacity of 692 mAh g^{-1} for the CTS@RGO paper was achieved after 100 cycles at a constant current density of 1000 mA g^{-1} (Figure S6). More importantly, the hybrid CTS@RGO paper as anode exhibits a high capacity and an excellent cycling stability compared with that of Cu_2SnS_3, SnS_2 and SnS_2/graphene electrodes at a constant current density of 500 mA g^{-1} (Figure S7–9). To the best of our knowledge, such a superior cycle performance of the copper tin sulfide/graphene has not been reported before (table S1). The outstanding electrochemical

performance of hybrid CTS@RGO paper can be attributed to its unique structure and lower stoichiometric of Cu.

For a better understanding of the advantage of Sn-based binary metal sulfides compared with single metal sulfides for LIBs, the EIS measurements of SnS_2 and Cu_2SnS_3 were performed, respectively. Whether before cycling or after 50 cycles, the impedance value of the SnS_2 is highest and the Cu_2SnS_3 is lowest in the three materials (Figure 6 and Figure S10), which is attributed to formation of Cu in the Cu_2SnS_3 and CTS to enhanced electronic conductivity. In addition, Figure S11 showed the photographs of the cycled wafer electrodes of the SnS_2, Cu_2SnS_3 and CTS under the same condition. After 10 cycles, the exposed current collector of SnS_2 electrode was clearly observed own to the exfoliation of active materials. In comparison, the cycled Cu_2SnS_3 and CTS electrodes kept intact, which can be attributed to presence of Cu in the Cu_2SnS_3 and CTS as inert matrix to mitigate the volume changes during the cycling process.

3. Conclusions

In conclusion, the self-standing and binder-free hybrid CTS@RGO paper has been successfully prepared via a simple sulfuration treatment of a hybrid mixture $CuSn(OH)_6$ submicron spheres and GO nanosheets. The hybrid CTS@RGO paper as anode for LIBs exhibits an excellent electrochemical performance compared with that of pristine CTS powder, including favorable capacity retention, good rate capability and high initial coulombic efficiency. Such outstanding Li ion storage property of the hybrid CTS@RGO paper originated from the unique sandwiches configuration and binder-free paper electrode fabrication method. Furthermore, the introduction of graphene in hybrid CTS@RGO paper not only improves electronic conductivity, but also acts as buffer to accommodate large volume changes and maintain electrode integrity during cycling. The results demonstrate that the hybrid CTS@RGO paper can promote the application of Sn-based anode material for LIBs.

Experimental Section

Materials Synthesis

All reagents were analytical grade and used as received without further purification. Firstly, graphite oxide (GO) was prepared by a modified Hummers method.[8] Then, $CuSn(OH)_6$ submicron spheres were prepared as precursor for CTS via a simple liquid phase method with water as solvent at room temperature.[28] Specifically, 2 mL concentrated ammonia solution was slowly added to 32 mL 0.05 M $CuSO_4$ solution and a dark blue solution was obtained. Then, 32 mL 0.05 M Na_2SnO_3 solution was added dropwise to the above solution and the mixed solution was stirred constantly for 20 min. The resultant precipitates of $CuSn(OH)_6$ were collected by centrifugation and washed with deionized water several times until pH value reached 7 and then were dried in vacuum oven at 60 °C for 24 h. Subsequently, 80 mg of $CuSn(OH)_6$ mixed with 20 mg of GO in 20 ml distilled water and then this suspension was treated by ultrasonication for 1 h. Afterwards, the sonication suspension was filtrated under the assistance of vacuum through a hydrophilic membrane (50 mm diameter, 450 nm pore size), followed by lyophilization. After that, this filtrated $CuSn(OH)_6$@GO paper was annealed with sublimed sulfur at 500 °C for 4 h under argon atmosphere. The final product of binder-free hybrid CTS@RGO paper was obtained. For comparison, CTS powder was prepared in similar process by direct annealing $CuSn(OH)_6$ submicron spheres with sublimed sulfur. The SnS_2, SnS_2/graphene and Cu_2SnS_3 were prepared by the same method reported in the previously literatures.[11b,29]

Materials Characterization

X-ray diffraction (XRD) patterns of the samples were collected by a Bruker-AXS Micro-diffractometer (D8 ADVANCE) with Cu K_α radiation ($\lambda = 1.5406$ Å). The Raman spectra of the samples were obtained on a Thermo Scientific DXRxi Raman system using 532 nm Ar-ion laser. The elemental chemical surface electronic environment details of the hybrid CTS@RGO paper were examined using X-ray photoelectron spectroscopy (XPS, ESCALab 220i-XL, VG Scientific) with Al K_α radiation (1486.6 eV). The morphologies of samples were characterized by field-emission scanning electron microscopy (FESEM, HITACHI S-4800).The scanning transmission electron microscopy (STEM) images were taken on field-emission transmission electron microscope (FETEM, TECNAI F30 G^2). The energy dispersive X-ray spectroscopy (EDS) mapping were determined by an EDAX system. Measurements of graphene content are performed with a thermogravimetric analysis (TGA) in air with a heating rate of 10 °C min^{-1} from room temperature to 900 °C.

Electrochemical Tests

The hybrid CTS@RGO paper was punched into a circular pellet with a diameter of 8 mm and which was directly used as anode for electrochemical test. The mass loading of the CTS@RGO paper was ca. 1.8 mg cm^{-2}. For comparison, the as-synthesized CTS powder was mixed with Super-P and poly(acrylic) acid binder (wt.% = 8:1:1) to form slurry followed by pasting the slurry onto copper foil and dried at 120 °C for 24 h under vacuum. Then the copper foil with active material was punched into a circular pellet with a diameter of 14 mm used as anodes for LIBs. All electrodes were assembled into CR2032 coin-type cells in an argon-filled glove box. The lithium foil and polypropylene membrane (Celgard 2500) were used counter electrode and separator, respectively. The electrolyte consists of 1 M $LiPF_6$ salt dissolved in a solution (EC:DMC:EMC = 1:1:1 in volume) and 2 wt.% vinylene carbonate (VC) was used in the cells. The galvanostatic charge/discharge cycling and rate properties of samples were performed in the potential range of 0.005–3.0 V vs. Li/Li^+ under a desired current density. All the specific capacities measured were based on the total mass of hybrid CTS@RGO paper or pure CTS (excluding binder and conductive additives) in electrodes. The cyclic voltammetry (CV) were examined using an Zennium (Zahner, Germany) instrument at a scanning rate of 0.2 mV s^{-1} with the potential ranging from 0.005 V to 3 V vs. Li/Li^+.

Acknowledgements

The authors thank the National Natural Science Foundation of China Program (No. 21473228, 51502319), the Shandong Provincial Natural Science Foundation (BS2015CL014), the Think-Tank Mutual Fund of Qingdao Energy Storage Industry Scientific

Research, and the Qingdao Key Lab of Solar Energy Utilization and Energy Storage Technology.

Conflict of Interest

The authors declare no conflict of interest.

Keywords: graphene buffer · high-capacity · lithium-ion batteries · Sn-based sulfides · volume variation

[1] a) M. Armand, J. Tarascon, *Nature* **2008**, *452*, 652–657; b) R. Verrelli, J. Hassoun, *ChemElectroChem* **2015**, *2*, 988–994; c) Z. Wang, M. Wang, Z. Yang, Y. Bai, Y. Ma, G. Wang, Y. Huang, X. Li, *ChemElectroChem* **2016**. DOI: 10.1002/celc.201600594.
[2] G. Lee, J. Kim, D. Lee, S. Seo, H. Shim, D. Kim, *ChemElectroChem* **2014**, *1*, 673–678.
[3] X. Xu, W. Liu, Y. Kim, J. Cho, *Nano Today* **2014**, *9*, 604–630.
[4] a) M. He, L. Yuan, Y. Huang, *RSC Adv.* **2013**, *3*, 3374; b) H. Tian, F. Xin, X. Wang, W. He, W. Han, *Journal of Materiomics* **2015**, *1*, 153–169; c) W. Ren, D. Kong, C. Cheng, *ChemElectroChem* **2014**, *1*, 2064–2069. d) J. Ye, T. Chen, Q. Chen, W. Chen, Z. Yu, S. Xu, *J. Mater. Chem. A* **2016**, *4*, 13194–13202; e) Q. Chen, F. Lu, Y. Xia, H. Wang, X. Kuang, *J. Mater. Chem. A* **2017**. DOI: 10.1039/C7TA00236 J.
[5] a) Y. Yu, L. Gu, C. Wang, A. Dhanabalan, P. A. van Aken, J. Maier, *Angew. Chem. Int. Ed.* **2009**, *48*, 6485–6489; b) C. Wu, J. Maier, Y. Yu, *Adv. Funct. Mater.* **2015**, *25*, 3488–3496.
[6] a) X. Wu, Y. Guo, L. Wan, *Chem Asian J* **2013**, *8*, 1948–1958; b) M. He, L. Yuan, X. Hu, W. Zhang, J. Shu, Y. Huang, *Nanoscale* **2013**, *5*, 3298–3305. c) Z. Liu, H. Bai, D. D. Sun, *Chem Asian J* **2012**, *7*, 2381–2385.
[7] a) G. Cui, Y. Hu, L. Zhi, D. Wu, I. Lieberwirth, J. Maier, K. Mullen, *Small* **2007**, *3*, 2066–2069; b) W. Xu, X. Cui, Z. Xie, G. Dietrich, Y. Wang, *ChemElectroChem* **2016**, *3*, 1098–1106; c) C. Zhu, P. Kopold, W. Li, P. A. van Aken, J. Maier, Y. Yu, *Adv. Sci.* **2015**, *2*, 1500200.
[8] G. Zhou, L. Yin, D. Wang, L. Li, S. Pei, I. R. Gentle, F. Li, H. Cheng, *ACS Nano* **2013**, *7*, 5367–5375.
[9] a) L. Zhang, L. Jiang, H. Yan, W. Wang, W. Wang, W. Song, Y. Guo, L. Wan, *J. Mater. Chem.* **2010**, *20*, 5462; b) X. Zhou, L. Wan, Y. Guo, *Adv. Mater.* **2013**, *25*, 2152–2157; c) A. M. Tripathi, S. Mitra, *ChemElectroChem* **2014**, *1*, 1327–1337; d) B. Qu, G. Ji, B. Ding, M. Lu, W. Chen, J. Y. Lee, *ChemElectroChem* **2015**, *2*, 1138–1143.
[10] M. Zhang, T. Wang, G. Cao, *Inter.Mater. Rev.* **2015**, *60*, 330–352.
[11] a) B. Qu, M. Zhang, D. Lei, Y. Zeng, Y. Chen, L. Chen, Q. Li, Y. Wang, T. Wang, *Nanoscale* **2011**, *3*, 3646–3651; b) B. Qu, H. Li, M. Zhang, L. Mei, L. Chen, Y. Wang, Q. Li, T. Wang, *Nanoscale* **2011**, *3*, 4389–4393.
[12] a) Q. Jiang, X. Chen, H. Gao, C. Feng, Z. Guo, *Electrochim. Acta* **2016**, *190*, 703–712; b) Z. Dong, R. Zhang, D. Ji, N. A. Chernova, K. Karki, S. Sallis, L. Piper, M. S. Whittingham, *Adv. Sci.* **2016**, *3*, 1500229; c) L. Fu, C. Zhang, B. Chen, Z. Zhang, X. Wang, J. Zhao, J. He, H. Du, G. Cui, *Inorg. Chem. Front.* **2017**. DOI: 10.1039/C6QI00521G.
[13] C. Villevieille, P. Novak, *J. Electrochem. Soc.* **2014**, *162*, A284–A287.
[14] F. Yan, X. Tang, Y. Wei, L. Chen, G. Cao, M. Zhang, T. Wang, *J. Mater. Chem. A* **2015**, *3*, 12672–12679.
[15] S. H. Choi, K. Y. Jung, Y. C. Kang, *ACS Appl. Mater. Interfaces* **2015**, *7*, 13952–13959.
[16] T. Lui, F. Hung, T. Lui, K. Chen, *J. Nanomater.* **2015**, *2015*, 1–7.
[17] J. Tang, J. Yang, L. Zhou, J. Xie, G. Chen, X. Zhou, *J. Mater. Chem. A* **2014**, *2*, 6292.
[18] H. Tao, S. Zhu, L. Xiong, X. Yang, L. Zhang, *ChemElectroChem* **2016**, *3*, 1063–1071.
[19] a) S. Stankovich, D. A. Dikin, R. D. Piner, K. A. Kohlhaas, A. Kleinhammes, Y. Jia, Y. Wu, S. T. Nguyen, R. S. Ruoff, *Carbon* **2007**, *45*, 1558–1565; b) Y. Yang, J. Li, D. Chen, T. Fu, D. Sun, J. Zhao, *ChemElectroChem* **2016**, *3*, 757–763.
[20] I. Y. Jeon, S. Zhang, L. Zhang, H. J. Choi, J. M. Seo, Z. Xia, L. Dai, J. B. Baek, *Adv. Mater.* **2013**, *25*, 6138–6145.
[21] a) W. Ai, Z. Luo, J. Jiang, J. Zhu, Z. Du, Z. Fan, L. Xie, H. Zhang, W. Huang, T. Yu, *Adv. Mater.* **2014**, *26*, 6186–6192; b) W. Lu, X. Gong, M. Nan, Y. Liu, S. Shuang, C. Dong, *Anal Chim Acta* **2015**, *898*, 116–127.
[22] S. S. Mali, B. M. Patil, C. A. Betty, P. N. Bhosale, Y. W. Oh, S. R. Jadkar, R. S. Devan, Y. Ma, P. S. Patil, *Electrochim. Acta* **2012**, *66*, 216–221.
[23] a) H. Tao, S. Zhu, X. Yang, L. Zhang, S. Ni, *J. Electroanal. Chem.* **2016**, *760*, 127–134; b) Z. Zhang, C. Zhou, M. Jia, Y. Fu, J. Li, Y. Lai, *Electrochim. Acta* **2014**, *143*, 305–311; c) L. Nie, Y. Zhang, K. Ye, J. Han, Y. Wang, G. Rakesh, Y. Li, R. Xu, Q. Yan, Q. Zhang, *J. Mater. Chem. A* **2015**, *3*, 19410–19416.
[24] H. Wan, G. Peng, X. Yao, J. Yang, P. Cui, X. Xu, *Energy Storage Mater.* **2016**, *4*, 59–65.
[25] Z. Zhang, Y. Fu, C. Zhou, J. Li, Y. Lai, *Solid State Ionics* **2015**, *269*, 62–66.
[26] Z. Wu, W. Ren, L. Wen, L. Gao, J. Zhao, Z. Chen, G. zhou, F. Li, H. Cheng, *ACS Nano* **2011**, *5*, 5463–5471.
[27] S. Xu, C. M. Hessel, H. Ren, R. Yu, Q. Jin, M. Yang, H. Zhao, D. Wang, *Energy Environ. Sci.* **2014**, *7*, 632–637.
[28] R. Xu, B. Deng, L. Min, H. Xu, S. Zhong, *Mater. Lett.* **2011**, *65*, 733–735.
[29] S. Liu, X. Lu, J. Xie, G. Cao, T. Zhu, X. Zhao, *ACS Appl. Mater. Interfaces* **2013**, *5*, 1588–1595.

Manuscript received: January 27, 2017
Accepted Article published: February 2, 2017
Final Article published: February 28, 2017